Available online at www.sciencedirect.com
SCIENCE DIRECT®
Precambrian Research 123 (2003) 135–157
Precambrian Research
www.elsevier.com/locate/precamres

Finite strain pattern in Andriamena unit (north-central Madagascar): evidence for late Neoproterozoic–Cambrian thrusting during continental convergence

Philippe Goncalves [a,*], Christian Nicollet [a], Jean-Marc Lardeaux [b]

[a] *Laboratoire Magmas et Volcans, Université Blaise Pascal-CNRS 5, rue Kessler, 63 038 Clermont-Ferrand cedex, France*
[b] *Laboratoire de Dynamique de la Lithosphère, Université Claude Bernard-CNRS 27, boulevard du 11 Novembre, 69 622 Villeurbanne cedex, France*

Accepted 20 November 2001

Abstract

This paper deals with the late Neoproterozoic–Cambrian tectonic evolution of a part of north-central Madagascar, which is characterized by the occurrence of a mafic-ultramafic sequence (the Andriamena unit) overlying a gneissic-granitic basement. The finite strain pattern has been determined by carrying out a SPOT satellite image analysis, structural mapping of specific areas and kinematic analyses of shear zones. Structural investigations reveal the presence of two superposed finite strain patterns, D_1 and D_2. The D_1 event is related to the emplacement of the Andriamena unit on the top of the gneissic-granitic basement. The western contact between these units is a major mylonitic zone characterized by a non-coaxial strain regime consistent with a top-to-east displacement. We suggest that the Andriamena unit originated as a lower crustal fragment of a middle Neoproterozoic continental magmatic arc related to the closure of the Mozambique Ocean. This fragment was thrusted onto the gneissic-granitic basement after 630 Ma, i.e. the age of emplacement of characteristic stratoid granites found only in the lower unit. The D_2 event is related to east-west horizontal shortening mainly accommodated by F_2 upright folds. In-situ electron microprobe dating of monazites from the Andriamena unit constrains the age of the D_1 and D_2 events between 530 and 500 Ma under amphibolite to granulite-facies conditions (5–7 kbar, 650–700 °C). The eastward thrust emplacement of the Andriamena unit (D_1) followed by the horizontal shortening (D_2) are ascribed to the same Cambrian tectonic regime (i.e. east-west convergence). Such D_1–D_2 bulk strain pattern has been recognized throughout Madagascar and at various structural levels of the crust: in the lower crust in Southern Madagascar and in the uppermost crustal level in the SQC unit (central Madagascar). The D_1–D_2 event is interpreted to result from the continental convergence of the Australia–Antarctica block and the Madagascar, India, Sri Lanka block during the final amalgamation of Gondwana.

Keywords: Madagascar; Mozambique Belt; Crustal shortening; Thrust; Electron microprobe dating; Monazite

1. Introduction

Knowledge of the timing of structural evolution is fundamental for understanding orogenic processes

* Corresponding author. Present address: Department of Geosciences, University of Massachusetts, 611, North Pleasent Street, AMHERST, MA 01003-9297, USA. Fax: +33-4-73-34-67-44.
E-mail address: philippe@geo.umass.edu (P. Goncalves).

0301-9268/03/$ – see front matter © 2003 Elsevier Science B.V. All rights reserved.
doi:10.1016/S0301-9268(03)00065-2

in collision zones. Thus, direct coupling of geochronological data with structural and petrologic information is essential to unravel the evolution of a huge orogenic belt like the Mozambique Belt. Before Mesozoic opening of the Mozambique channel, Madagascar was located adjacent to Kenya and Tanzania, close to the eastern front of the Mozambique Belt. The recognition of important variations in ages of peak-metamorphic conditions across the Mozambique Belt has demonstrated that such belt does not simply result from the collision of the supercontinents East and West Gondwana. It was rather formed by multiple collisions of continent, micro-continent and arc terranes during Neoproterozoic (Stern, 1994; Meert and Van der Voo, 1997). Consequently, it is fundamental to recognize and constrain the geometry and timing of collision zones that bound these accreted terranes. In north-central Madagascar, the identification of juxtaposed crustal blocks, including the Andriamena unit, with contrasted lithological, metamorphic and geochronological characteristics (Bésairie, 1963; Collins and Windley, in press) raises the problem of how and when these tectonic blocks accreted. The Andriamena unit is known to have crucial geodynamic significance in the Precambrian evolution of Madagascar, owing to the occurrence of late Archaean UHT metamorphism (Nicollet, 1990; Goncalves et al., 2000, 2001) and middle Neoproterozoic intrusive gabbros. These rocks have been interpreted as remnants of the root of a continental magmatic arc (Guérrot et al., 1993; Handke et al., 1999).

The aim of this paper is to constrain the structural evolution of a part of north-central Madagascar. Numerous geochronological studies have recently been performed in this area (Caen-Vachette, 1979; Guérrot et al., 1993; Nicollet et al., 1997; Paquette and Nédélec, 1998; Tucker et al., 1999; Kröner et al., 2000; Goncalves et al., 2000), but almost no modern structural studies have been done, except in the area of the stratoid granites west of Andriamena (Nédélec et al., 1994) and in the Antananarivo virgation area (Nédélec et al., 2000). Combining the structural data with *P–T* metamorphic estimates and in-situ geochronology, we discuss the thermo-tectonic evolution of a portion of the north-central Malagasy basement, including the Andriamena unit.

2. Geological setting

The Malagasy basement is classically divided into two parts. The southern part, south of the Bongolava-Ranotsara shear zone (Fig. 1) is characterized by a generalized late Neoproterozoic tectonothermal imprint with no record of Archaean ages (Andriamarofahatra et al., 1990; Paquette et al., 1994; Kröner et al., 1996; Montel et al., 1996; Nicollet et al., 1997; Martelat et al., 2000; de Wit et al., 2001). The finite strain pattern results in the superposition of two Neoproterozoic deformation events D_1 and D_2, which are characterized by a flat-lying foliation (S_1) bearing an east-west lineation (L_1) and by a network of kilometer-scale vertical shear zones (S_2) bounding folded domains (Fig. 1). The D_2 structures have been interpreted as the result of late Neoproterozoic east-west horizontal shortening in a transpressive regime under granulite-facies conditions (see discussions in Pili et al., 1997; Martelat et al., 1997, 2000).

Since the 1970s and the studies of Bésairie (1963) two main lithological units have been recognized in north-central Madagascar: a basement mainly composed of late Archaean (~2.5 Ga) granitoids and migmatitic gneisses containing a significant Neoproterozoic juvenile component (Tucker et al., 1999; Kröner et al., 2000; the Antananarivo block of Collins et al., 2000), which is structurally overlain by a late Archaean mafic sequence. This latter sequence occurs as three north-south elongated units, named respectively from west to east: Maevatanana, Andriamena, and Aloatra–Beforona (Fig. 1). They are interpreted as a part of the same lithostratigraphic unit: the "Beforona group" of Bésairie (1963) or the same tectonic unit: the "Tsaratanana thrust sheet" of Collins et al. (2000). Our study is focussed on the Andriamena mafic unit and the surrounding gneissic-granitic basement.

Geochronological results show that the late Archaean basement and the mafic sequence record a complex Neoproterozoic polymetamorphic and magmatic history (Guérrot et al., 1993; Nicollet et al., 1997; Paquette and Nédélec, 1998; Tucker et al., 1999; Kröner et al., 2000; Goncalves et al., 2000). A widespread and voluminous magmatic activity is characterized by the emplacement of gabbroic and granitoid rocks at ~820–720 Ma (Guérrot et al., 1993; Tucker et al., 1999; Kröner et al., 2000). This Neoproterozoic igneous activity, which also affected the

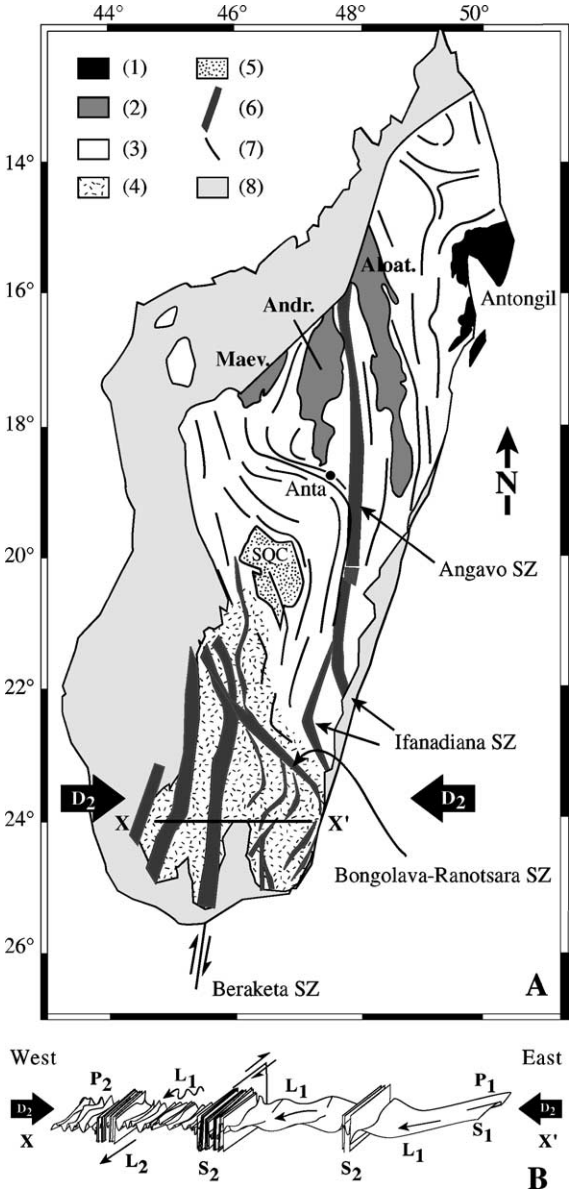

Fig. 1. (A) Simplified geological map of Madagascar, with the main structural features (modified after Martelat, 1998), highlighting the north-south trending structures. In southern Madagascar, the deformation is related to an east-west horizontal shortening (D_2). (1) Middle and late Archaean gneisses and granitoids, (2) late Archaean and Neoproterozoic mafic gneisses and metapelites, (3) late Archaean and Neoproterozoic gneisses and granitoids (the gneissic-granitic basement in the text), (4) late Neoproterozoic granulite-facies metabasites and metapelites, (5) greenschist-amphibolite-facies metasedimentary rocks and middle Neoproterozoic intrusions (SQC unit), (6) late Neoproterozoic–Cambrian shear zones, (7) major structural trend, (8) late Paleozoic–Mesozoic sediments and volcanic rocks, Maev.: Maevatanana unit, Andr.: Andriamena unit, Aloat.: Aloatra–Beforona unit, Anta: Antananarivo. (B) Schematic cross-section of southern Madagascar showing the main structures related to the D_1 and D_2 tectonic event (Martelat et al., 1999).

SQC unit (Schisto-Quartzo-Calcaire unit or alternatively named Itremo Group) of central Madagascar (see location in Fig. 1), is interpreted as the result of continental arc magmatism related to the closure of the Mozambique Ocean at about the same time as the break-up of the supercontinent Rodinia (Tucker et al., 1999; Handke et al., 1999). North-west of Antananarivo, the late Archaean gneissic basement was intruded under LP–HT conditions by the "stratoid granites" at 630 Ma (Paquette and Nédélec, 1998). Finally, the finite strain pattern observed in north-central Madagascar is related to a late Neoproterozoic tectonic event (Kröner et al., 2000; Nédélec et al., 2000), contemporaneous with a period of high-grade metamorphism and intrusive igneous activity (580–520 Ma; Tucker et al., 1999; Kröner et al., 2000).

2.1. The Andriamena unit

The Andriamena unit located north of Antananarivo (see location in Fig. 2), consists mainly of interlayered mafic and tonalitic gneisses (biotite-hornblende and biotite gneisses), metapelitic migmatites (garnet-sillimanite bearing rocks) and quartzites associated with numerous large, deformed, mafic to ultramafic bodies. These mafic bodies include dunites, peridotites and pyroxenites associated with chromite mineralizations and gabbros equilibrated under *P–T* conditions of about 4–5 kbar, 500–800 °C and with preserved igneous textures (Cocherie et al., 1991; Guérrot et al., 1993). The few available geochronological data highlight the high-grade polymetamorphic evolution of the Andriamena unit between late Archaean to Neoproterozoic times (Guérrot et al., 1993; Nicollet et al., 1997; Goncalves et al., 2000). Relict high Al–Mg granulites preserve ultra-high temperature assemblages (garnet-sapphirine-quartz, orthopyroxene-sillimanite-quartz), suggesting minimal *P–T* conditions of about 11 kbar and 1050 °C, which have been dated at 2.5 Ga using electron microprobe dating of monazites (Nicollet, 1990; Nicollet et al., 1997; Goncalves et al., 2000). A second

Fig. 2. Simplified geological map with the foliation trajectories obtained from seven SPOT satellite images and 1/100,000 geological maps. (1) Gneissic-granitic basement, (2) Andriamena unit (mafic gneisses, biotite gneisses, migmatites), (3) mafic-ultramafic intrusions, (4) U–Pb ages from the stratoid granites (Paquette and Nédélec, 1998), and (5) Pb–Pb evaporation ages from granites, and hornblende-biotite gneiss (Kröner et al., 2000).

widespread granulitic event, coeval with partial melting, occurred at peak conditions of about 850 °C, 6–7 kbar and has been dated to about 730–770 Ma (Nicollet et al., 1997; Goncalves et al., 2000). This second granulitic event could be associated with the emplacement of the mafic-ultramafic intrusions at 787 ± 16 Ma (Guérrot et al., 1993; Goncalves et al., 2000). Finally, the Andriamena unit was reworked with the rest of Madagascar during late Neoproterozoic times.

2.2. The gneissic-granitic basement

The basement in north-central Madagascar, and more particularly west and south-west of the Andriamena unit, is composed mainly of alternating layers with variable thicknesses of biotite-hornblende-rich gneisses locally associated with sillimanite-bearing metapelites and alkaline granites (stratoid or sheet-like granites). These granites have been interpreted as syntectonic granites emplaced at 630 Ma in a post-collisional extensional setting (Nédélec et al., 1994; Paquette and Nédélec, 1998). However, such specific tectonic setting is poorly constrained and remain unclear. Indeed, post-collisional extension should be associated with a regional high temperature metamorphism. Up to now, this 630 Ma event has been recognized only in the stratoid granites located west of the Andriamena unit and in one intrusive hornblende-granodiorite gneiss located within the Aloatra–Beforona unit, east of Antananarivo (637 ± 1 Ma; Tucker et al., 1999). Another uncertainty exists about the real timing of their emplacement. Indeed, near Antananarivo, Paquette and Nédélec (1998) have dated a stratoid granite at 627 ± 2 Ma using U–Pb zircon method (sample MG 65). In contrast about 15 km south-east, Kröner et al. (2000), obtained a mean $^{207}Pb/^{206}Pb$ age of 764 ± 1 Ma from a sample (MAD 80) interpreted by Kröner et al. (2000) as a "charnockite partly retrogressed into a granite-gneiss." According to the outcrop features and the petrography, we suggest that this partly retrogressed charnockite corresponds to a stratoid granite similar to the one dated by Paquette and Nédélec (1998). This assumption is also well supported by the major and trace element composition of sample MAD 80 (Kröner et al., 2000) which is consistent with the mildly alkaline suite defined by Nédélec et al. (1995) and from which sample MG 65 is derived. Thus, the recognition of contradictory ages for emplacement of the stratoid granites led us to be very careful with subsequent tectonic interpretations.

3. Strain pattern and related structures

3.1. Method

The finite strain pattern was derived from the study of satellite images (seven SPOT scenes; Table 1), combined with the analysis of the geological maps (scale 1/100,000) and field investigations. Such combined approach has been successfully used in southern Madagascar to deduce the crustal-scale finite strain pattern (Martelat et al., 1995, 1997, 2000) and allow an analysis at various scales. Satellite imagery was also used to propose a consistent large-scale structural map integrating the Andriamena unit to north-central Madagascar.

The map of foliation trajectories (Fig. 2) outlines a clear predominance of N160°–N180° directions, and more particularly in the Andriamena unit where these directions are accentuated by the north-south elongate shape of the Andriamena unit and the mafic-ultramafic bodies in the northern part of studied area. These

Table 1
Reference and scene center location of the seven SPOT satellite images used to draw the map of foliation trajectories (Fig. 2)

KJ	SPOT	Date	Spectral mode	Scene center location
168–385	4	98/06/20	XI	−17°31′11″/47°17′25″
169–385	4	98/07/21	XI	−17°31′11″/47°44′43″
168–386	4	98/06/20	XI	−18°01′09″/47°10′36″
168–386	2	99/10/02	XS	−18°29′47″/47°00′20″
169–387	4	98/07/21	XI	−18°31′07″/47°31′36″
168–387	2	96/04/10	XS	−18°56′30″/47°07′20″
169–388	4	98/07/21	XI	−19°01′04″/47°47′25″

directions are consistent with the general orientation of the main late Neoproterozoic structures observed at the scale of Madagascar (Fig. 1). In the gneissic-granitic basement, the trajectories of the regional foliation are more irregular and define complex folded and elliptical structures. South of the study area, near Antananarivo, the foliation trajectories form a complex pattern that includes the east-west trending of the Antananarivo virgation, the north-south Angavo shear zone and the highly folded domains close to the Carion granite and north of Mahitsy (Fig. 2). Our study is mainly focussed in the northern part of Fig. 2, where two different domains have been defined with respect to their lithological and structural characteristics: The Andriamena unit (Fig. 3a and b) and the gneissic-granitic basement, which is illustrated by Fig. 6 for the western Kiangara area and Fig. 7 for the eastern Ambakireny area.

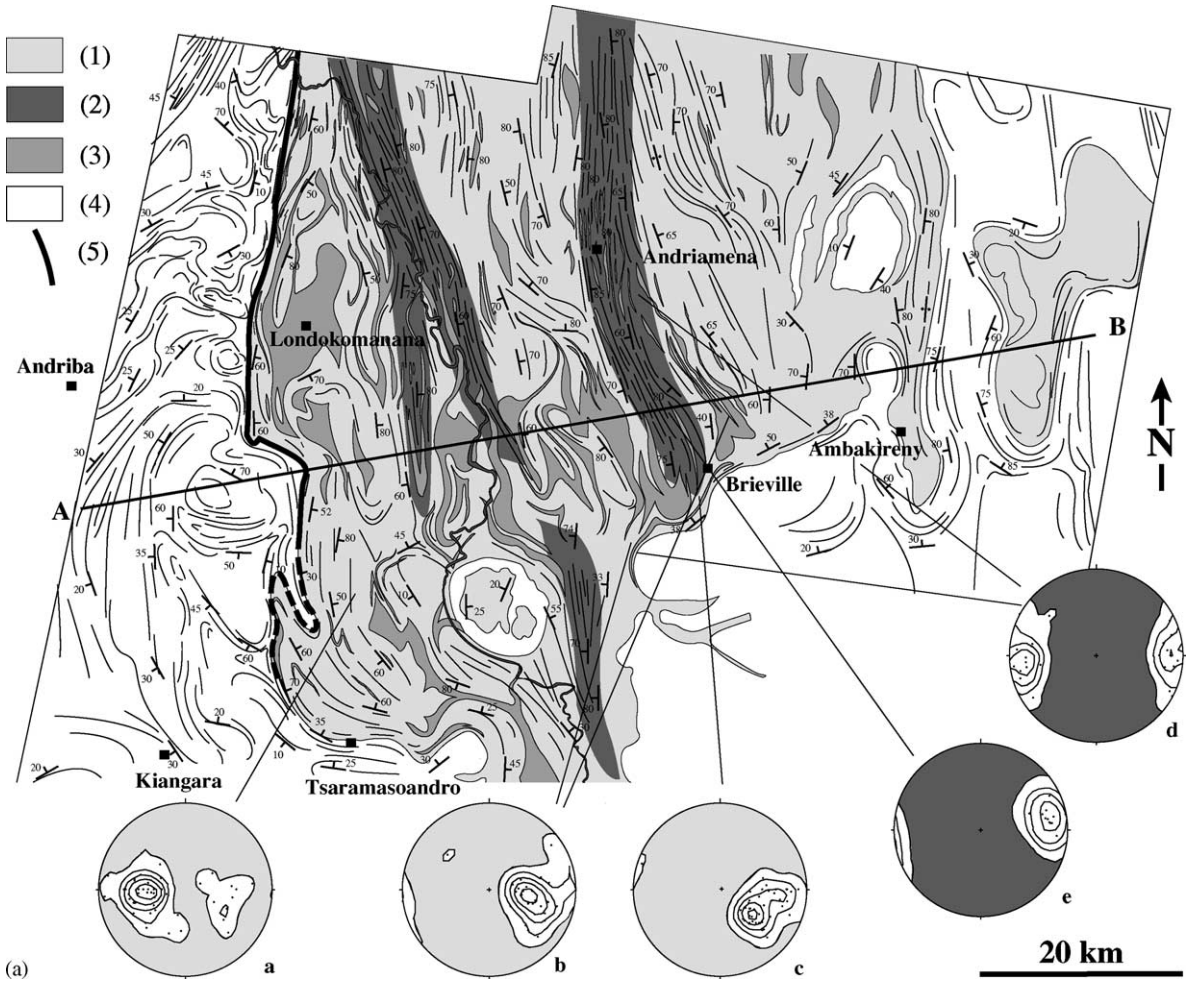

Fig. 3. (a) Map of foliation trajectories in the central Andriamena unit (from our field investigations and 1/100,000 geological maps). (1) D_2 low-strain zone, (2) D_2 high-strain zone, (3) mafic-ultramafic intrusions, (4) gneissic-granitic basement, and (5) mylonitic zone. Equal area stereograms with projection onto the lower hemisphere: for the low-strain zones (a) 47 data, (b) 31 data, (c) 41 data; for the high-strain zones (d) 24 data, (e) 12 data. (b) Map of mineral lineation trajectories and F_1–F_2 fold axes in the central Andriamena unit. Equal area stereograms with projection onto the lower hemisphere: for the low-strain zones (a) 48 data, (b) 31 data, (c) 41 data; for the high-strain zones (d) 28 data, (e) 11 data. (1) D_2 low-strain zone, (2) D_2 high-strain zone, (3) mafic-ultramafic intrusions, (4) gneissic-granitic basement, (5) lineations from Nédélec et al. (1994), and (6) lineations from this work, numbers refer to plunge amount.

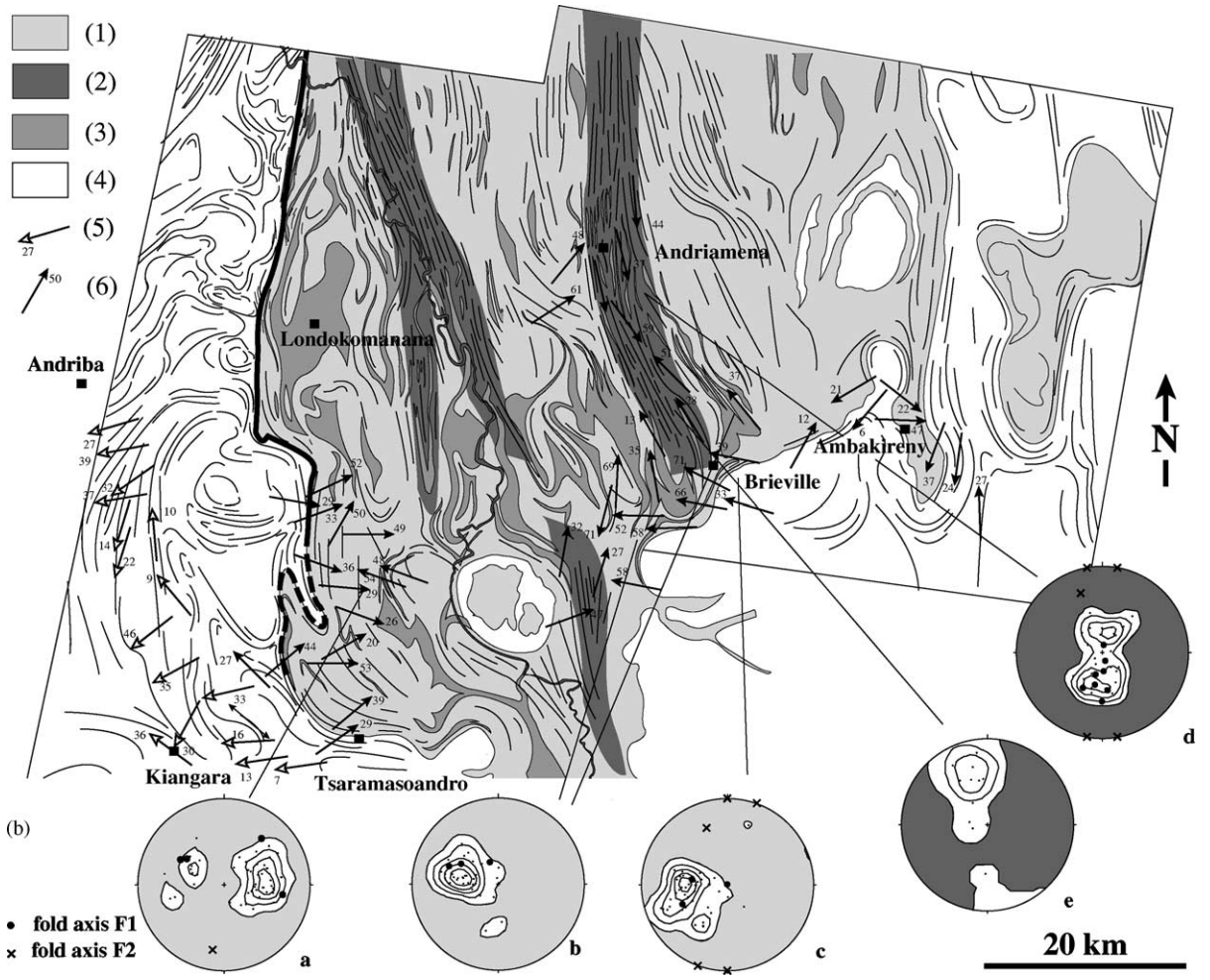

Fig. 3. (*Continued*).

3.2. The Andriamena unit

The foliation in the Andriamena unit corresponds to a gneissic layering composed by parallel layers of mafic and quartzofeldspathic gneisses and mafic-ultramafic bodies. At the regional scale, the foliation plane, denoted as S_1, is folded at various scales by F_2 folds with steeply dipping north-south axial planes and sub-horizontal axes (Fig. 3b (stereonets a, c, d and 4)). The N160°–N180° trending structures (Fig. 3a) and the north-south synformal structure of the Andriamena unit (Fig. 4) are related to such (F_2) folding, which is consistent with east-west horizontal shortening (D_2). The D_2 deformation is heterogeneous and shows strain partitioning between extensive low-strain zones (zones in light grey in Fig. 3a and b) bounded by an anastomosing network of high-strain zones dominantly oriented N160°–N180° with widths up to 10 km (zones in dark grey in Fig. 3a and b). In the low-strain zones, the S_1 foliation and the mafic-ultramafic intrusions are gently folded by F_2 kilometer-scale open folds, without any related axial plane foliation (Fig. 3a, b and 4). Locally, granite veins intrude parallel to the F_2 axial planes. In the high-strain zones, the foliation is sub-vertical (Fig. 3a (stereonets d and e)) and was formed either by the rotation of S_1 to vertical or by the formation of a second penetrative foliation (S_2). Mafic-ultramafic intrusions

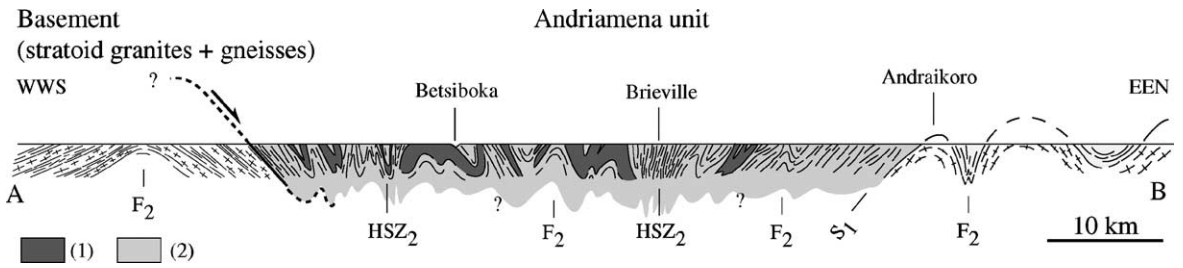

Fig. 4. Cross-section showing the F_2 open to upright folds affecting the S_1 foliation in the Andriamena unit and the stratoid granites. The F_2 folds also affect the mafic-ultramafic intrusions. The western mylonitic contact between the Andriamena unit and the gneissic-granitic basement shows a top-to-east sense of shear. (1) Neoproterozoic mafic-ultramafic intrusions, (2) mafic and quartzofeldspathic gneisses of the Andriamena unit, HSZ_2: high-strain zone (D_2). For location see Fig. 3a.

located in the high-strain zones are characterized by high aspect ratios ($10 < H/L < 40$) consistent with strong sub-horizontal shortening (D_2) in these zones (Fig. 3a).

In the low-strain zones, where D_2 strain is moderate, the L_1 stretching lineation, marked by biotite or amphibole, defines a regular east-west trend, perpendicular to the Andriamena/basement contact, with a pitch around 90° (Fig. 3b (stereonets a, b, and c)). In the high-strain zones, where the S_1 foliation is rotated to vertical, the L_1 lineations are steeply plunging due to their passive rotation during the F_2 folding (Fig. 3b (stereonet d)). Near Brieville, where S_1 is transposed into a new foliation (S_2), the L_1 lineation is replaced by a new sub-horizontal lineation (L_2) broadly oriented N170 (Fig. 3b (stereonet e)).

Structures related to the D_1 deformation can be observed more easily outside the D_2 high-strain zones. At the outcrop scale, numerous isoclinal intrafolial folds occur with hinges parallel to the L_1 lineation and sub-horizontal axial planes (Fig. 3b (stereonets a, b, c and 5)). The initially horizontal S_1 foliation is also affected by boudinage compatible with the east-west stretching lineation direction (Fig. 5). All these structures suggest that the D_1 event included a significant amount of vertical shortening. The D_2 high-strain zones are characterized by numerous upright F_2 folds, which locally deform the F_1 isoclinal folds. The lack of asymmetric structures in the zones characterized by intense transposition, as shown by the very high aspect ratio of the mafic-ultramafic bodies, is consistent with a strong component of coaxial strain associated with a horizontal east-west shortening during the D_2 event.

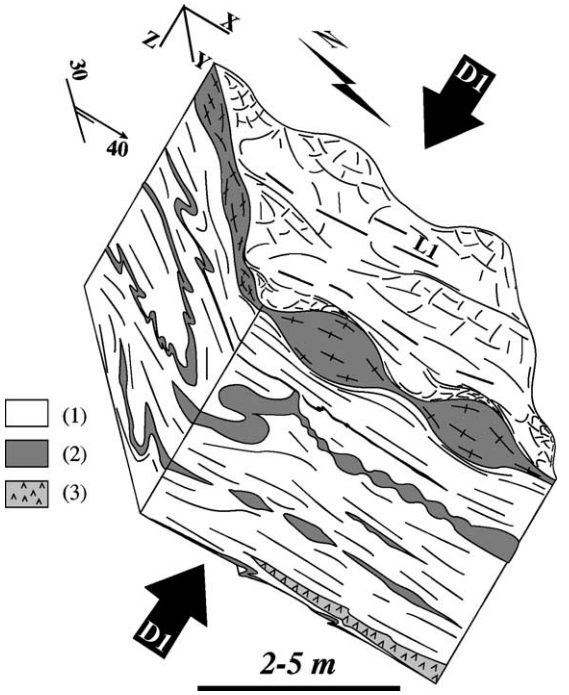

Fig. 5. Schematic block diagram showing the different types of structures related to the D_1 event, at outcrop scale. In the YZ section: isoclinal folds with axes parallel to the L_1 lineation; in the XZ section: boudinage structures associated with scarce folds with axes perpendicular to the L_1 lineation; in the XY section: chocolate-block boudinage surface with a lineation L_1. All these structures are consistent with a vertical shortening. The actual orientation of the block diagram is related to the later D_2 folding. (1) biotite gneiss, (2) pegmatite, and (3) metabasite.

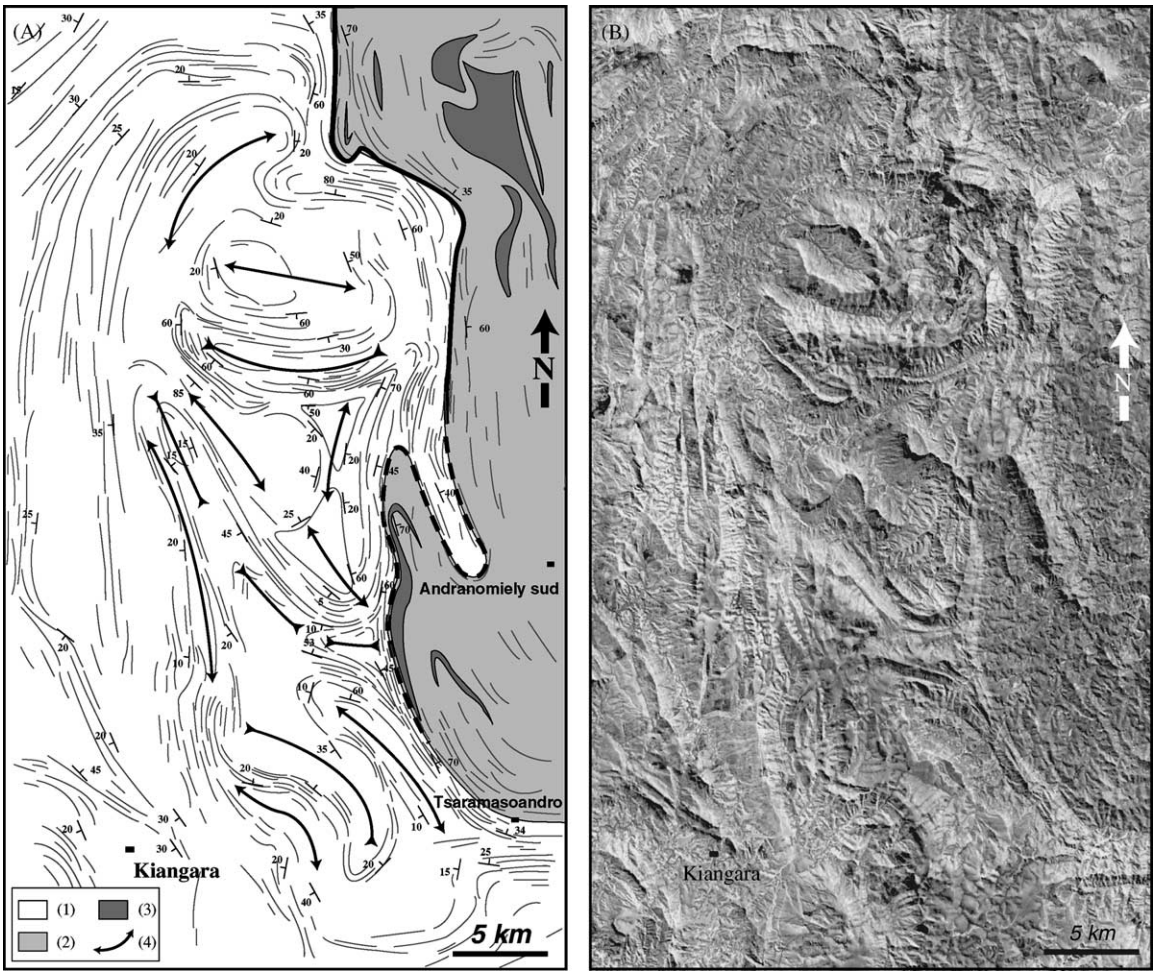

Fig. 6. (A) Detailed map of foliation trajectories with fold axial traces defining type II fold-interference patterns, in the Kiangara area. (1) Gneissic-granitic basement, (2) Andriamena unit, (3) mafic-ultramafic intrusions, and (4) fold axial traces. (B) Part of the SPOT satellite images 168–385 and 168–386.

3.3. The gneissic-granitic basement

3.3.1. The Kiangara area: large-scale type II fold-interference patterns

In the western Kiangara area (Figs. 2 and 6), the foliation in the basement is defined by an alternation, at various scales, of gneisses with foliation parallel stratoid granites. Close to Andriba and Kiangara, the structural pattern is characterized by a constant and west dipping foliation bearing a sub-horizontal WSW trending lineation (Fig. 3a and b; Nédélec et al., 1994). The foliation and its mineral lineation have been interpreted as magmatic structures developed during the emplacement of the magma under amphibolitic-facies conditions (4–5 kbar and ~750 °C) at 630 Ma (Paquette and Nédélec, 1998).

A highly complex fold pattern domain of 15 km in width is observed from satellite images, bounded at the east by the Andriamena unit and at the west by the monoclinal stratoid granites (Fig. 3a and 6). The foliation trajectories define kilometric “boomerang” structures (Fig. 6) typical of type II fold-interference patterns (Ramsay, 1967). The axial trace of the late generation is oriented N150°–N180° (Fig. 6) and corresponds to open folds with vertical axial planes and sub-horizontal axes. These folds are consistent

with the F_2 folding event defined in the Andriamena unit. The first fold generation, which have not been observed at the outcrop scale, should correspond to kilometric isoclinal folds with gently dipping axial planes and N90° axes according to the type II fold-interference pattern model (Ramsay, 1967). Such orientation is consistent with axial trace oriented N90° in Fig. 6.

3.3.2. *The Ambakireny area: dome-and-basin structures*

The Ambakireny area is located east of the Andriamena unit and is bounded at the east by the north-south Angavo shear zone (Fig. 2). The S_1 regional foliation pattern in this area defines typical dome-and-basin structures (Fig. 7). The main features are:

(1) The S_1 foliation is parallel to the lithologic contact between the mafic gneisses (Andriamena unit) and the underlying gneissic and granitic basement. Furthermore, the dense mafic gneisses of the Andriamena unit are systematically located in the basins whereas the less dense gneissic basement defines the domes.

(2) In the foliation map (Fig. 7), we observe that the structures are elliptical with their long axis oriented N160°–N180° (Fig. 7). In the central parts of the gneissic domes, the foliation is sub-horizontal and becomes steeper at the boundaries. In the basins, where the mafic gneisses crop out, the foliation is sub-vertical and folded by the upright F_2 folds with north-south steeply dipping axial planes and sub-horizontal axes (Fig. 4). This folding, as well as the elliptical shape of the structures, is in agreement with the D_2 regional east-west horizontal shortening inferred from the Andriamena unit structures.

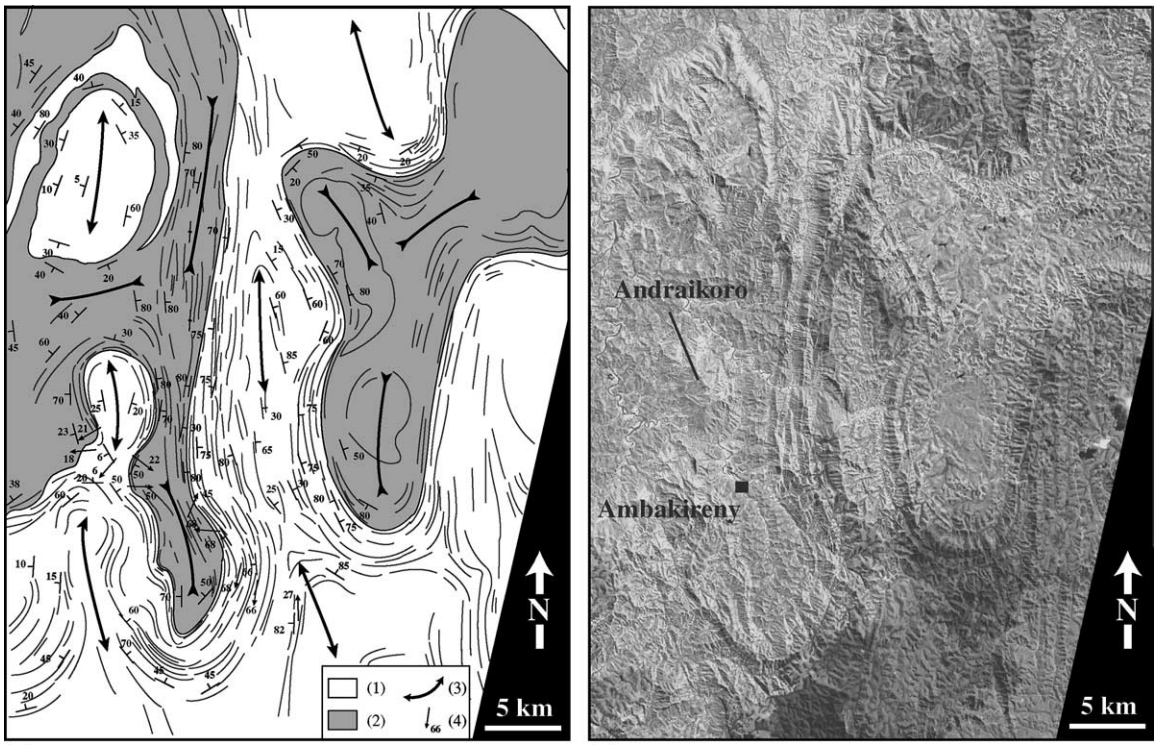

Fig. 7. (A) Detailed map of foliation and lineation trajectories with fold axial traces defining dome-and-basin structures in the Ambakireny area. The denser mafic gneisses of Andriamena are systematically located in the basins while the granitoids form the domes. Note the elliptical shape of the structures consistent with an east-west horizontal shortening. (1) Gneissic-granitic basement, (2) mafic gneisses of the Andriamena unit, (3) fold axial traces, and (4) stretching lineations. (B) Part of the SPOT satellite image 169–385.

(3) The contacts between the Andriamena unit and the underlying basement are generally steeply dipping, but close to the synformal closures they shallow out. There is an increase in strain as the contact is approached, but no kinematic indicators were observed here. Locally, around the Andraikoro dome, just north of Ambakireny, the steeply plunging lineations display a radial pattern broadly centered on the core of the dome (Fig. 7).

The main feature observed here is the predominance of F_2 folding. The superposition of such folds on an earlier fold generation with east-west vertical axial surfaces and horizontal axes, can yield dome-and-basin fold-interference pattern (type I from Ramsay, 1967). However, we cannot ruled out that the high-density contrast between the mafic gneisses of the Andriamena unit located in the basins and the granitic rocks of the basement forming the domes could also favor the formation of dome-and-basin structures by relative vertical displacements resulting from gravitational instabilities.

3.4. The western Andriamena/basement contact: a major mylonitic zone

A major mylonitic zone occurs between the Andriamena unit and the underlying gneissic-granitic basement (Fig. 3a). This north-south trending structure extends over more than 200 km, suggesting

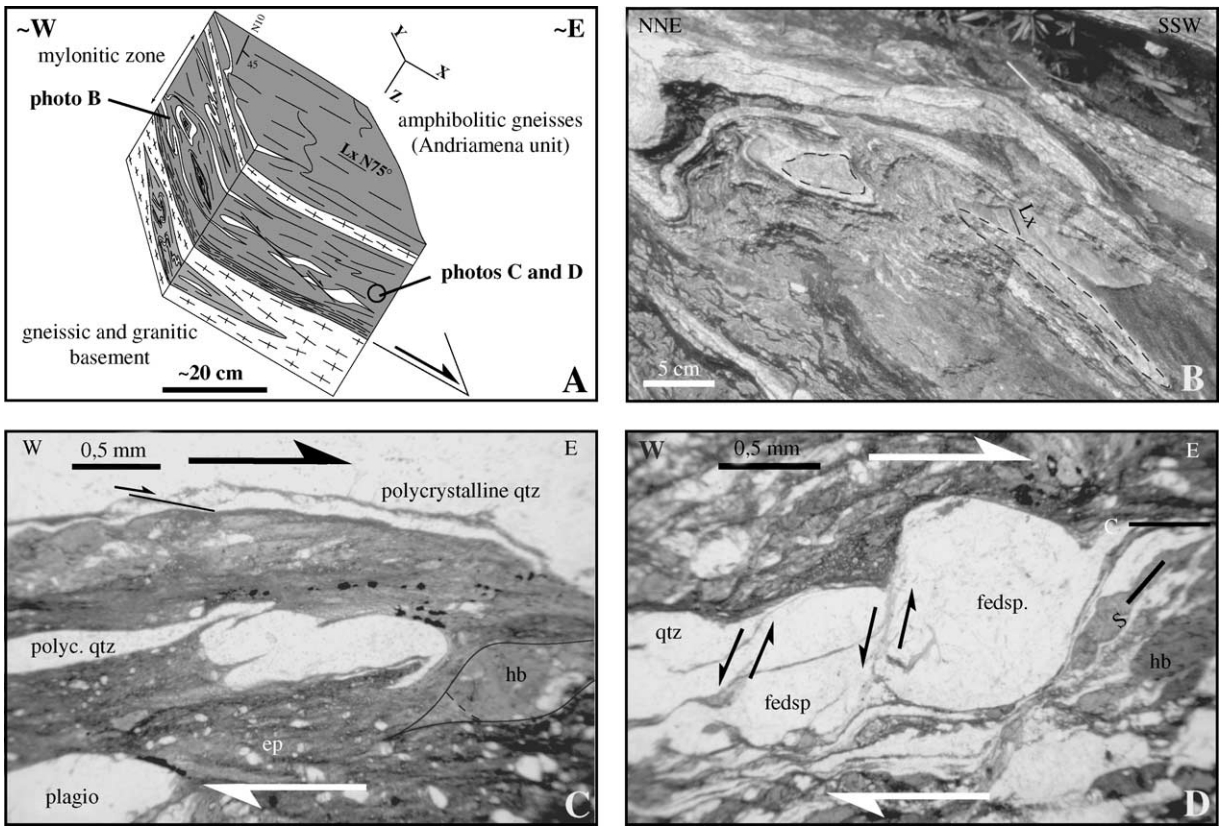

Fig. 8. The basal mylonitic Andriamena/basement contact. All the kinematic indicators are consistent with a top-to-east sense of shear. (A) Schematic block diagram showing the various structures observed in all the sections of the finite strain ellipsoid. (B) Outcrop view of the YZ section of the strain ellipsoid showing sheath-folds consistent with a high-strain regime at the Andriamena/basement contact. (C) Microstructures observed in thin-sections parallel to the lineation (XZ section of the strain ellipsoid). The asymmetric microfolds associated with the σ and C/S type structures imply a non-coaxial strain regime consistent with a top-to-east sense of shear. (D) Fractured feldspar porphyroclast in thin-section in the XZ plane of the strain ellipsoid, indicating antithetic shears within a top-to-east shear zone.

that the Andriamena/basement contact acted as a major deformation zone during the tectonic evolution of north-central Madagascar. It lies parallel to S_1 foliation, dipping east (Fig. 4), with a thickness ranging from one to several meters. The stretching lineation associated with the mylonitic foliation is defined by the elongation of quartz aggregates and the preferred orientation of syn-kinematic biotite and plunges east.

Numerous kinematic indicators occurring at various scales, including sheath folds developed in the YZ section of the finite strain ellipsoid, C/S structures, asymmetric microfolds, and asymmetric boudins in the XZ section (Fig. 8), indicate a non-coaxial deformation regime (Fig. 8). The sense of shear in the mylonitic zone is consistent a top-to-east sense of shear. The late folding (D_2 event) of this contact impede a direct kinematic interpretation of these shear sense indicators.

The mylonite is composed of a quartzite-phyllite alternation at centimeter-scale. The metamorphic mineral assemblage (hornblende + feldspar + epidote + biotite and quartz) is compatible with deformation under epidote-amphibolite-facies conditions and probably until greenschist-facies conditions. Quartzite layers are composed of elongate monocrystalline quartz ribbons with undulatory extinction, and/or polycrystalline quartz ribbons. The micaceous layers contain rounded fragments of feldspar, which are locally disrupted by antithetic shears (Fig. 8).

4. Metamorphism and geochronology of the Andriamena unit

Petrology of migmatites, metapelites and associated metabasites has been investigated in order to estimate the regional conditions of metamorphism in the study area. Geochronologic constraints have been carried out using electron microprobe dating technique on migmatites and metapelites from distinct structural positions in the Andriamena unit.

In-situ chemical U–Th–Pb ages and the associated statistical treatment follow the analytical procedure detailed by Montel et al. (1996). Analyses were performed directly on thin-sections on a Cameca SX100 electron microprobe at the laboratoire Magmas et Volcans of Clermont-Ferrand, France. Individual ages were calculated from the U, Th, and Pb concentrations assuming that non-radiogenic lead in the monazite is negligible. The 2σ errors given on individual ages are calculated by propagating the uncertainties on U, Th, and Pb concentrations (with 95% confidence level) into the decay equation of Montel et al. (1996). According to the relatively less precision with respect to isotopic methods, numerous ages are obtained in a single crystal or thin-section, in order to obtain a statistical confident age. The age population is graphically presented in weighted histogram representation corresponding the sum of all individual ages and their uncertainties represented by bell-shaped probability curves. The calculated mean age and its associated error (with 95% confidence level) is based on a least-squares modeling, which allows to identify eventual multiple age populations. The quality of the modeling is assessed from the mean square weighted deviation (MSWD).

4.1. Migmatites and metapelites

Migmatite C98 sampled about 10 km southwest of Brieville (Fig. 9), outside the D_2 high-strain zones, consists of alternating melanosomes and leucosomes which correspond to the gneissic layering (S_1). The melanosome is composed of centimeter-sized resorbed garnet porphyroblast, biotite, sillimanite, plagioclase, and quartz. Biotite occurs either as small inclusions in garnet porphyroblasts or as euhedral crystals up to 1 mm forming aggregates with large sillimanite dispersed in the matrix or around garnet. The leucosome is characterized by the presence of aggregates of perfectly euhedral muscovite associated with biotite and sillimanite, dispersed in a matrix composed of quartz and plagioclase. Garnet is scarce and occurs as strongly resorbed grains. According to the NaKFMASH petrogenetic grid of Spear et al. (1999), the lack of K–feldspar in the both layers and crystallization of hydrous phases like biotite + muscovite with sillimanite at the expense of garnet and crystallizing from melt, implies a cooling under *P–T* conditions of 4–7 kbar at 650–700 °C. Temperatures estimated with various calibrations of the Fe–Mg exchange garnet-biotite geothermometer on garnet rim and matrix biotite are highly variable, but remain consistent with the petrogenetic grid constraints. For instance, temperatures calculated with the calibration of Ferry and Spear (1978) are between

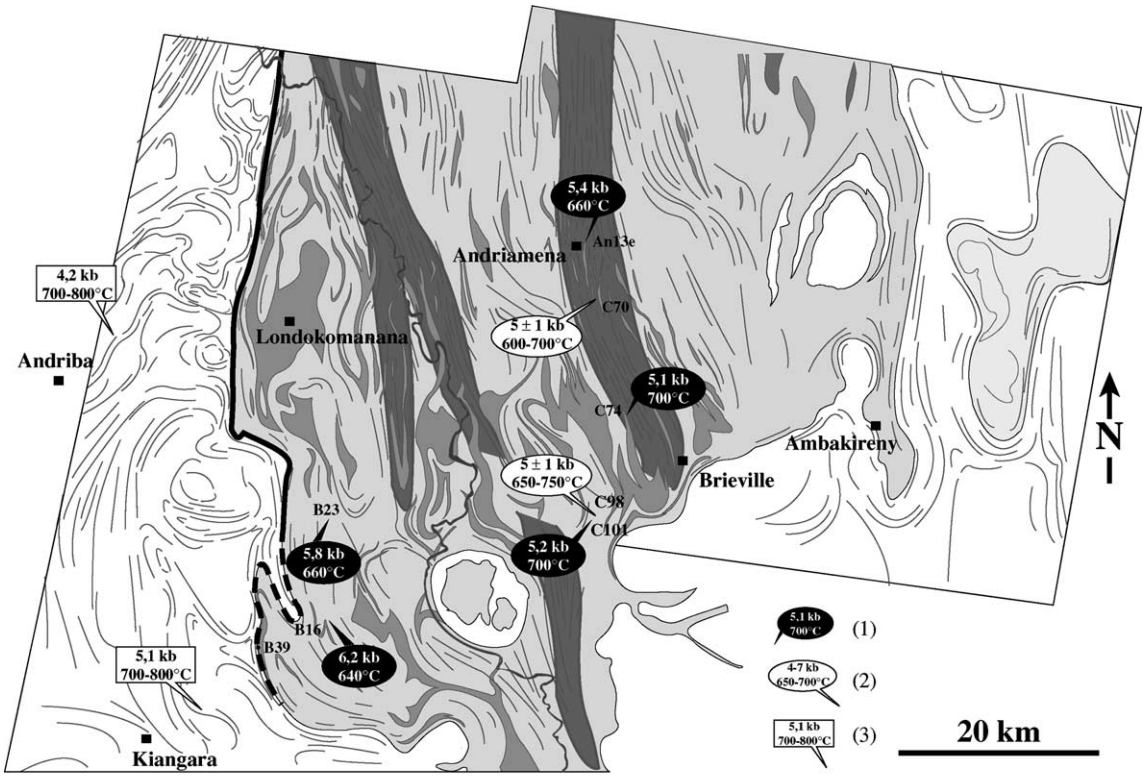

Fig. 9. Sample locations and *P–T* conditions. (1) Metabasites, (2) migmatites and metapelites, and (3) migmatites and stratoid granodiorite from Nédélec et al. (1994).

700–840 °C in the melanosome and 660–720 °C in the leucosome. Pressure of the cooling path estimated with the garnet-sillimanite-plagioclase-quartz barometer (Hodges and Crowley, 1985; Koziol, 1989) or the garnet-plagioclase-biotite-muscovite-quartz, ranges between 4.8 ± 0.1 and 6.1 ± 0.2 kbar (at 700 °C). This result is consistent with the pressure estimated from the NaKFMASH petrogenetic grid.

Monazites occur predominantly in the melanosome as sub-euhedral grains from 40 to ~100 μm in size with well-developed crystal faces (Fig. 10a). They are systematically located in the matrix and are in textural equilibrium with the metamorphic assemblage. It suggests that monazite growth is coeval with partial melting. Backscattered electron images do not reveal clear zoning (Fig. 10a). Thirty-six analyses have been carried out in six grains. Monazites are characterized by very low ThO_2 and UO_2 concentrations (<2.9 and <0.3 wt.%) and in some grains, the Pb contents are below the detection limit (<130 ppm; Table 2). Twenty-five calculated individual ages range between 342 ± 120 and 561 ± 181 Ma and define an unimodal population at 499 ± 19 Ma (MSWD = 0.56; Figs. 11a and 12). The large errors on individual ages are related to the very low lead contents. The euhedral morphology of most of the monazite grains, and the unimodal age population, suggests that the age of 499 ± 19 Ma is the age of partial melting.

Migmatite B39 was collected very close to the western Andriamena/basement contact (Fig. 9). Such sample displays a gneissic foliation, involving leucosomes and aligned biotite, which is parallel to the major mylonite zone. Furthermore, stretching lineation in sample B39, which is marked by the preferred orientation of biotite, is also consistent with the mylonitic lineation related to the D_1 event. The migmatite consists of strongly resorbed garnet, euhedral biotite, plagioclase, K–feldspar, and elongated

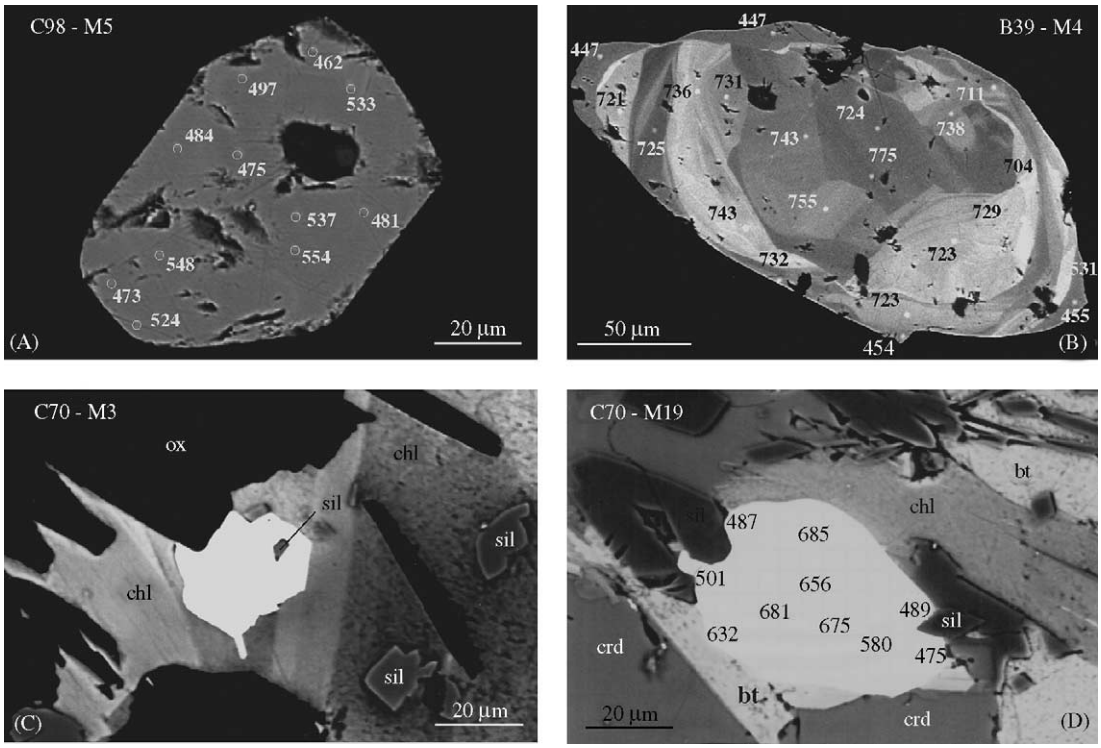

Fig. 10. Backscattered electron image of selected monazite grains of sample C98, B39, and C70. Circles or white dots mark the position of electron microprobe analyses labeled with measured age in million years. (A) Euhedral unzoned monazite from a migmatite (sample C98) yielding a mean age of 499 ± 19 Ma (2σ errors for each individual ages is about 100 Ma), (B) monazite from a migmatite (sample B39) exhibiting a complex internal patchy zoning which is truncated by secondray overgrowths in the rim. Core of the grain yields a calculated mean age of 724 ± 5 Ma whereas, overgrowths yield systematically youngest ages of 457 ± 7 Ma (2σ errors for each individual ages is about 25 Ma), (C) euhedral monazites from metapelite (C70) containing an inclusion of sillimanite and in textural equilibrium with chlorite formed during the cooling stage. Such monazite (M3) yields a mean age of 501 ± 10 Ma, and (D) sub-euhedral monazite from metapelite (C70) showing textural evidences of its final growth sub-contemporaneous with the crystallization of the euhedral sillimanites formed during the cooling stage. Calculated individual ages range from 685 Ma in the core to 475 Ma in the rims (2σ errors for each individual ages is about 50 Ma).

quartz parallel to the biotite foliation. Garnet contains rounded inclusions of spinel, sillimanite, quartz, ilmenite, and scarce biotite, which are never in mutual contact. Due to the relatively poor mineralogy, *P–T* estimates cannot be constrained. Temperature of the retrograde evolution calculated with the garnet-biotite geothermometer of Ferry and Spear (1978) using garnet rim and matrix biotite are about $740 \pm 40\,^{\circ}C$.

Two distinct populations of monazites have been observed: (1) small monazites (10–20 μm) in textural equilibrium with aggregates of biotite forming the S_1 foliation. (2) large elliptical monazites (100–200 μm) located in the matrix and aligned with the main foliation (S_1). Back-scattered electron imaging reveals in some large-grain complex internal patchy zoning, truncated by secondary domains at the grain margins (Fig. 10b). Such rims have been observed in all grains either as irregular narrow domains or small overgrowths (<10 μm) with well-developed crystalline faces. Both populations of monazite grains can also been distinguished according to their ThO_2 content. Indeed, the small monazites grains associated with the biotite are characterized by the lowest ThO_2 contents (<4.1 wt.%), whereas the large grains (including the cores and the secondary overgrowths) have significantly higher ThO_2 contents (in M4: $9.4 < ThO_2 < 14.4$ wt.%). UO_2 content of the both groups is very low (<0.3 wt.%) leading a Th/U ratio

Table 2
U–Th–Pb electron microprobe analyses and calculated individual ages from migmatite C98

Crystal	Analyses	Th (ppm)	U (ppm)	Pb (ppm)	Time (Ma)
M1	37	14250 ± 401	1900 ± 166	480 ± 67	519 ± 95
	38	5320 ± 327	990 ± 161	<D.L.	n.d.
	39	7710 ± 346	570 ± 161	<D.L.	n.d.
	40	17580 ± 421	1650 ± 164	520 ± 69	502 ± 86
	41	9620 ± 364	2760 ± 170	370 ± 68	441 ± 100
	42	19770 ± 436	2430 ± 170	640 ± 69	511 ± 71
	43	14920 ± 406	2180 ± 168	500 ± 67	503 ± 87
	44	25580 ± 473	2570 ± 171	720 ± 69	471 ± 58
	45	11490 ± 375	1080 ± 164	230 ± 67	342 ± 120
	46	8990 ± 360	1540 ± 167	290 ± 68	459 ± 134
	47	7350 ± 345	530 ± 162	<D.L.	n.d.
M2	48	25260 ± 470	920 ± 163	640 ± 69	502 ± 71
M3	49	5890 ± 335	1990 ± 168	300 ± 68	534 ± 154
	50	3640 ± 312	2000 ± 167	230 ± 66	499 ± 179
	51	340 ± 289	3260 ± 172	250 ± 66	501 ± 163
M4	52	3250 ± 306	290 ± 156	<D.L.	n.d.
	53	3750 ± 313	660 ± 162	<D.L.	n.d.
	54	3260 ± 311	580 ± 162	<D.L.	n.d.
	55	1290 ± 289	1120 ± 164	<D.L.	n.d.
	56	2680 ± 305	860 ± 164	<D.L.	n.d.
	57	2510 ± 302	680 ± 163	<D.L.	n.d.
	59	6170 ± 334	1240 ± 164	260 ± 64	561 ± 181
	60	1900 ± 296	1200 ± 164	130 ± 63	494 ± 301
M5	62	12400 ± 386	910 ± 164	320 ± 66	462 ± 122
	63	24850 ± 470	930 ± 166	670 ± 69	533 ± 73
	64	20950 ± 447	1780 ± 167	600 ± 68	497 ± 74
	65	9280 ± 364	1640 ± 167	320 ± 66	484 ± 128
	66	12900 ± 388	2470 ± 169	520 ± 67	548 ± 93
	67	14630 ± 404	1470 ± 167	460 ± 68	524 ± 101
	68	2260 ± 300	2450 ± 168	220 ± 66	473 ± 175
	69	14850 ± 405	1890 ± 167	510 ± 68	537 ± 94
	70	9900 ± 366	2090 ± 168	420 ± 68	554 ± 116
	71	11930 ± 381	1980 ± 167	400 ± 67	481 ± 103
	72	13330 ± 394	2210 ± 169	440 ± 66	475 ± 91
M6	73	0 ± 0	1480 ± 164	<D.L.	n.d.
	74	270 ± 278	460 ± 161	<D.L.	n.d.

Errors at 2σ. <D.L.: below the detection limit. Backscattered image of monazite M5 is shown in Fig. 10a.

between 7–19 for the small monazites associated with the biotite and 37–85 for the large grains. Monazites associated with the biotite are also characterized by low lead contents, which is very close to the detection limit (~120 ppm; Table 3). Nine grains were analyzed yielding 88 individual ages, which range from 215 ± 92 to 775 ± 32 Ma (Table 3). Monazites associated with biotite also yield the youngest ages, until 215 ± 92 Ma. Due to the very low lead content, such ages must be considered with caution and were not used in the calculation of the mean ages. The weighted histogram clearly shows two main populations at 724 ± 5 Ma ($n = 62$) and 457 ± 7 Ma ($n = 19$; MSWD = 0.81) (Fig. 11b). The core of the large grains yield homogeneous middle Neoproterozoic ages without any relation with the zoning (Fig. 10b). We interpret the 724 ± 5 Ma age as the age of partial melting. The early Paleozoic ages were systematically recorded in the overgrowths (Fig. 10b) and in the small euhedral monazites associated with the biotite.

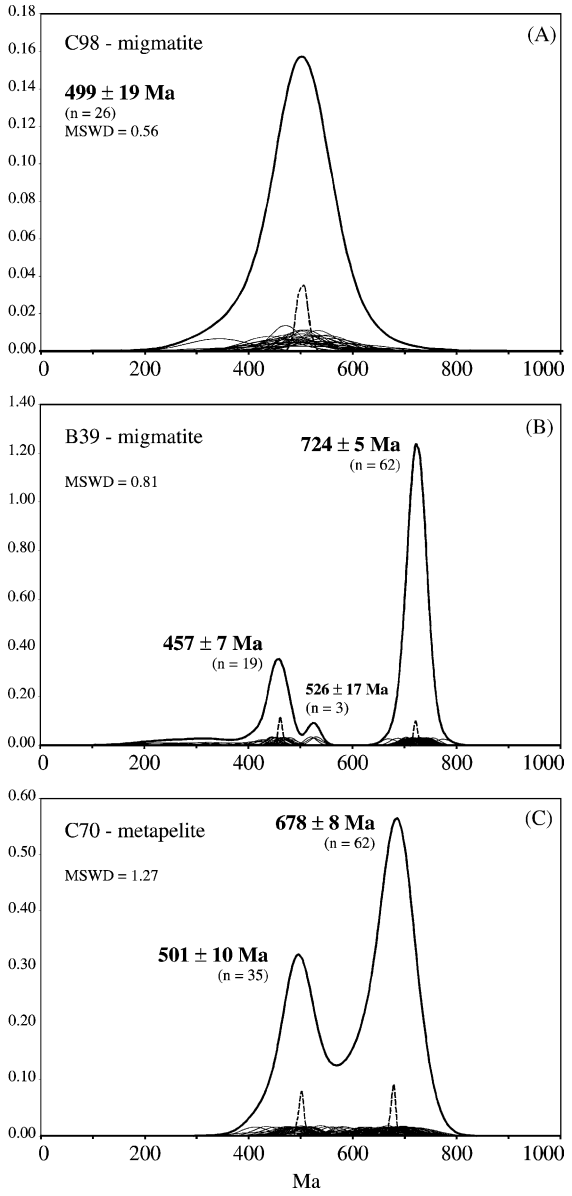

Fig. 11. Weighted histogram representation of the age data. Each small bell-shaped curve corresponds to Gaussian representation of individual age and its 2σ error calculated from U, Th, and Pb analysis. The thick curve corresponds to the sum of all small bell-shaped curves. The dotted curve is the statistically calculated mean age. There is no unit for vertical axe. (A) C98 migmatite located in a D_1 preserved area, (B) B39 migmatite located near the Andriamena/basement contact, and (C) C70 metapelite from a D_2 high-strain zone.

According to the microtextural features, we suggest that this Cambro–Ordovician age reflects the biotite crystallization. Finally, three individual ages define a poorly constrained population at about 526 ± 17 Ma (Fig. 11b).

Sample C70 is a metapelite collected about 5 km south of Andriamena, in a D_2 high-strain zone (Fig. 9). The outcrop is characterized by the development of a second penetrative foliation (S_2) at the expense of the previous S_1 foliation. Metapelite C70 is characterized by numerous local assemblages suitable to constrain the *P–T* evolution. It consists of few strongly resorbed garnet located in aggregates of cordierite, plagioclase, biotite, needles, or prismatic sillimanite ± chlorite. Cordierite is also associated with small euhedral staurolite, biotite, and sillimanite. Others domains are composed by abundant chlorite with needles of sillimanite and euhedral staurolite. Textural observations suggest the formation of the successive assemblages (quartz and plagioclase in excess): (1) grt-bt-sil; (2) grt-crd-bt-sil; (3) crd-bt-sil-st; (4) chl-sil-st. Such sequence of assemblages is consistent with a near-isobaric cooling from about 700 to 600 °C, at pressure of 5 ± 1 kbar, according to topology of the *P–T* grid for pelites in the KFMASH system (Spear, 1999).

The monazites of C70 are very abundant and usually occur as euhedral grains up to 50 μm with well defined faces. Microtextural features clearly indicate that the final growth of the monazites is sub-contemporaneous with chlorite, biotite, or sillimanite (Fig. 10c and d). Dates from the rims of monazites in textural equilibrium with the above-mentioned phases should correspond to the timing of the near-isobaric cooling under amphibolite-facies conditions. Back scattered imaging reveals in some grains a slight zoning, which consists of an inherited large core partly rimmed by secondary euhedral overgrowths. Eighteen monazites were analyzed yielding 98 measurements. Monazites are moderately radioactive and display very homogeneous ThO_2 and UO_2 contents (1.0–5.3 and 0.1–0.4 wt.%, respectively). Individual ages range continuously from 412 ± 51 to 734 ± 65 Ma but we can define two main age groups at 680 ± 8 and 501 ± 10 Ma (MSWD = 1.51). In contrast to sample B39 where the two distinct age populations (724 ± 5 and 457 ± 7 Ma) are clearly separated by a “age gap” of about 150 Ma, numerous intermediate ages lie between the 680 and

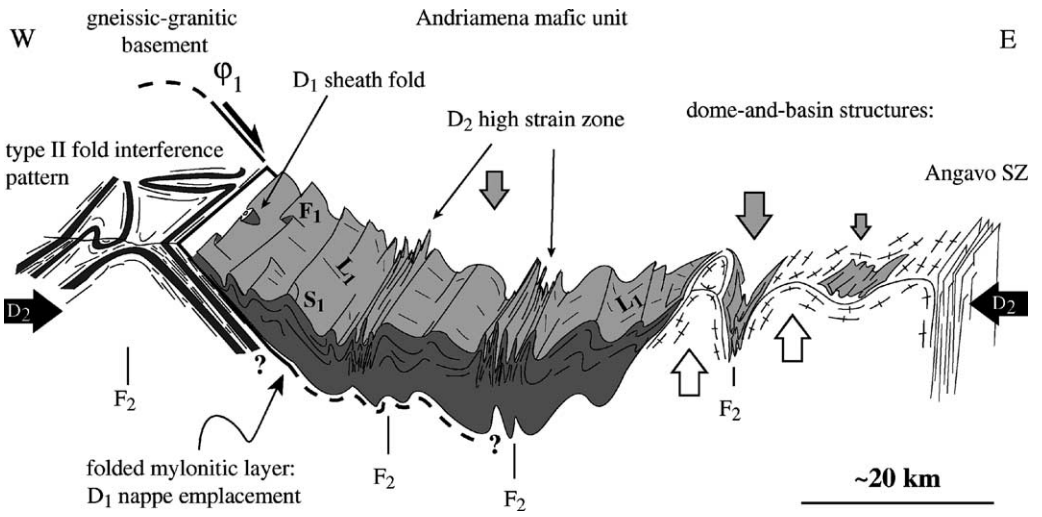

Fig. 12. Schematic E-W cross-section through the Andriamena unit showing the main structural features related to the D_1 and D_2 tectonic events. The D_1 structures (S_1 foliation bearing an east-west lineation (L_1), isoclinal folding (F_1) and sheath folds observed in the western mylonitic contact (φ_1) are related to Cambrian (530–500 Ma) top-to-east nappe emplacement of the Andriamena unit upon the gneissic-granitic basement. The D_1 structures have been reworked during the D_2 east-west horizontal shortening at about 500 Ma. The Angavo shear zone and F_2 folding, which also affects the stratoid granites, accommodate the D_2 shortening.

501 Ma population (Fig. 11b and c). Cambrian age (501 ± 10 Ma) was reported in euhedral monazites in equilibrium with chlorite (monazite M3; Fig. 10c and Table 4) and in rims or secondary overgrowths of monazites located in aggregates of cordierite, biotite, and staurolite (monazite M10, M16, M19; Fig. 10d). Such Cambrian age reflects a new episode of monazite crystallization during the near-isobaric cooling event, from about 700 to 600 °C, at pressure of 5 ± 1 kbar. Monazites which belong to the 680 Ma age group display a large age spreading, commonly exceeding 100 Ma, observed in a same grain (e.g. M10: from 441 ± 115 to 702 ± 62 Ma or M7: from 639 ± 55 to 727 ± 56 Ma; Table 4). The maximal age preserved in these monazites (734 ± 65 Ma) is consistent with the middle Neoproterozoic age obtained on the migmatite B39 (724 ± 5 Ma). Consequently we interpret the 680 Ma age populations as apparent ages which result of partial lead loss of 730 Ma old monazites during the Cambrian event.

4.2. Metabasites

Metamorphic conditions have been also evaluated using metabasites from the D_1 low-strain zones (samples B16, B23, and C101) and the D_2 high-strain zones (samples C74 and An13e) (Fig. 9). These metabasites are characterized by amphibolite-facies and granulite-facies assemblages (opx-cpx-grt-pl-qtz; opx-cpx-amph-pl-qtz). In these rocks, post-peak garnet coronas are produced by reactions like: opx + pl = cpx + grt + qtz; cpx + pl = grt + qtz; hb + pl = grt + qtz, which are indicative of near-isobaric cooling following peak granulite-facies metamorphism. Multi-equilibrium thermobarometric calculations (TWEEQU software, version 2.02; Berman, 1991) have been used on these coronas where the assumption of local chemical equilibrium is satisfied (Nicollet, 1988; St-Onge and Ijewliw, 1996). Average *P–T* estimates are 5–6 kbar and 650–700 °C and are homogeneous at the scale of the Andriamena unit (Fig. 9). These results are in good agreement with metamorphic conditions derived from the metapelites and migmatites. The age of these metabasites is unknown, but the occurrence of migmatites and metapelites dated at about 500 Ma displaying the same *P–T* conditions (e.g. migmatite C98 and metabasite C101) suggests that the amphibolite to granulite-facies conditions recorded in the metabasites of Andriamena are Cambrian (~500 Ma).

Table 3
U–Th–Pb electron microprobe analyses and calculated individual ages of selected monazites from migmatite B39

Crystal	Analyses	Th (ppm)	U (ppm)	Pb (ppm)	Time (Ma)
M1	1	29600 ± 495	1520 ± 166	650 ± 67	418 ± 55
M2	2	21220 ± 441	1510 ± 165	380 ± 64	324 ± 66
M5	3	11190 ± 376	1680 ± 165	160 ± 60	215 s± 92
M6	4	16330 ± 410	1440 ± 163	340 ± 65	360 ± 84
	5	15450 ± 403	1380 ± 163	260 ± 62	291 ± 83
M7	7	13470 ± 393	1000 ± 164	180 ± 60	240 ± 93
M11	21	35580 ± 526	1020 ± 164	730 ± 67	417 ± 49
M4	17	84130 ± 743	2000 ± 172	3190 ± 89	775 ± 32
	18	87460 ± 756	1970 ± 171	3080 ± 89	724 ± 30
	19	93050 ± 776	1620 ± 170	3290 ± 90	738 ± 29
	20	94490 ± 780	1320 ± 169	3180 ± 89	711 ± 29
	21	127080 ± 890	1620 ± 172	4220 ± 101	704 ± 24
	22	116720 ± 856	2000 ± 174	4070 ± 100	729 ± 25
	23	104140 ± 813	1590 ± 172	2620 ± 84	531 ± 23
	24	102060 ± 807	1400 ± 169	3490 ± 93	723 ± 28
	25	105340 ± 819	2100 ± 172	3780 ± 96	743 ± 27
	26	111830 ± 843	2590 ± 175	4120 ± 100	755 ± 26
	27	100140 ± 801	2170 ± 172	3610 ± 94	743 ± 28
	28	124500 ± 881	2070 ± 173	4420 ± 104	743 ± 25
	29	100800 ± 803	2300 ± 173	3590 ± 94	731 ± 28
	30	115870 ± 856	2420 ± 174	4130 ± 100	736 ± 26
	31	79800 ± 729	1100 ± 169	2740 ± 85	725 ± 33
	32	109860 ± 834	1380 ± 169	3730 ± 96	721 ± 26
	33	84600 ± 746	1540 ± 169	1800 ± 76	447 ± 25
	34	88310 ± 758	1480 ± 169	1870 ± 77	447 ± 24
	30′	84480 ± 745	1390 ± 170	1820 ± 76	455 ± 25
	31′	86140 ± 750	1610 ± 169	1870 ± 76	454 ± 24
	32′	93770 ± 778	1150 ± 167	3230 ± 90	731 ± 29

Monazites M1, M2, M5, M6, M7, M11 correspond to small grains in textural equilibrium with biotite. Monazite M4 is a large grain strongly zoned and showing small overgrowths (<10 μm) in the rims. Backscattered image of monazite M4 is shown in Fig. 10b.

5. Interpretation

The finite strain pattern and the structures recognized in a part of north-central Madagascar are the results from the superposition of two major episodes of deformation (D_1 and D_2). Structures related to the two events are summarized in Fig. 12.

5.1. D_1 event: Andriamena nappe emplacement

The D_1 event corresponds to the main fabric-forming event. D_1 structures consist of a sub-horizontal gneissic layering denoted as the S_1 foliation, bearing an east-west stretching lineation (L_1). This foliation is coeval with F_1 isoclinal folds with N90° horizontal axes parallel to the L_1 lineation (Fig. 12). Boudinage structures are consistent with the extension direction derived from the lineation (L_1). These structures are consistent with a sub-vertical shortening. Towards the contact with the underlying gneissic-granitic basement, in the western part of the Andriamena unit, the amount of finite strain increases and clear non-coaxial strain markers are observed in the major mylonitic zone, with a top-to-east shear sense (Fig. 12).

The Andriamena unit forms part of a mafic sequence (Maevatanana, Andriamena and Aloatra–Beforona) called by Collins et al. (2000) as the Tsaratanana thrust sheet. It is characterized by the occurrence of numerous middle Neoproterozoic intrusive mafic-ultramafic bodies that do not intrude the underlying

Table 4
U–Th–Pb electron microprobe analyses and calculated individual ages of selected monazites from metapelite C70

Crystal	Analyses		Th (ppm)	U (ppm)	Pb (ppm)	Time (Ma)
M3	2′	r	32500 ± 511	1490 ± 168	860 ± 67	510 ± 53
	3′	r	32400 ± 510	1530 ± 166	830 ± 67	493 ± 53
	4′	r	35640 ± 529	1830 ± 168	970 ± 68	517 ± 48
	5′	r	34180 ± 520	1580 ± 167	850 ± 66	479 ± 49
	1	c	33250 ± 516	1590 ± 168	860 ± 66	497 ± 51
	2	c	33480 ± 516	1500 ± 167	890 ± 67	514 ± 52
	3	r	36260 ± 531	1610 ± 168	950 ± 67	508 ± 48
M7	13′	r	33360 ± 515	1980 ± 169	1260 ± 69	697 ± 56
	8	c	38110 ± 541	1950 ± 170	1440 ± 70	713 ± 51
	9	c	40310 ± 554	1420 ± 166	1390 ± 70	683 ± 50
	10	c	34370 ± 523	1660 ± 168	1220 ± 69	676 ± 55
	11	c	30030 ± 500	2830 ± 172	1300 ± 69	727 ± 56
	12	c	41440 ± 560	1740 ± 169	1480 ± 71	693 ± 48
	13	r	31020 ± 503	2730 ± 172	1240 ± 69	684 ± 55
	14	r	31610 ± 507	2970 ± 172	1340 ± 70	713 ± 54
	15	c	35350 ± 526	1190 ± 164	1190 ± 68	670 ± 55
	16	r	29180 ± 492	1120 ± 166	1050 ± 67	706 ± 66
	17	r	35010 ± 525	1650 ± 168	1220 ± 69	667 ± 54
	18	r	34120 ± 521	1510 ± 167	1130 ± 68	639 ± 55
M10	20	o	30420 ± 500	1670 ± 168	800 ± 66	495 ± 54
	21	c	28020 ± 484	2010 ± 169	1020 ± 67	651 ± 61
	22	c	26110 ± 475	2560 ± 171	1100 ± 67	702 ± 62
	24	c	13710 ± 395	1610 ± 165	420 ± 63	491 ± 96
	25	c	10670 ± 371	1360 ± 165	300 ± 62	441 ± 115
	26	o	30470 ± 500	1520 ± 166	790 ± 66	495 ± 55
	27	r	16530 ± 410	2490 ± 169	710 ± 65	634 ± 80
	28	c	17060 ± 417	1460 ± 166	580 ± 64	587 ± 89
	29	c	13310 ± 391	1690 ± 166	530 ± 64	620 ± 103
	30	r	15200 ± 403	1690 ± 167	540 ± 64	575 ± 93
M16	38	o	43330 ± 567	1600 ± 167	1180 ± 69	539 ± 43
	39	c	31250 ± 507	1550 ± 167	1200 ± 68	727 ± 61
	40	c	34930 ± 525	1840 ± 168	1270 ± 69	684 ± 54
	41	r	40410 ± 553	2120 ± 169	1470 ± 71	684 ± 48
M19	21′	r	33810 ± 520	1600 ± 168	860 ± 66	489 ± 50
	22′	r	36360 ± 536	1460 ± 169	880 ± 66	475 ± 47
	23′	r	36100 ± 531	1380 ± 167	890 ± 67	487 ± 49
	24′	r	37640 ± 539	2040 ± 170	1000 ± 67	501 ± 45
	25′	r	27890 ± 486	1520 ± 168	940 ± 66	632 ± 63
	58	c	34140 ± 521	1680 ± 168	1230 ± 69	685 ± 55
	59	c	32910 ± 512	1270 ± 166	1100 ± 68	656 ± 58
	60	c	34990 ± 524	1090 ± 166	1190 ± 68	681 ± 57
	61	c	35560 ± 529	1620 ± 168	1250 ± 69	675 ± 54
	62	c	40050 ± 552	1530 ± 169	1180 ± 69	580 ± 47

Position of microprobe analyses; c: core.

gneissic-granitic basement. The lithologic contrast between the Andriamena unit and the basement and the high non-coaxial strain at the Andriamena/basement contact suggests that the Andriamena unit is an allochthonous unit with respect to the gneissic-granitic basement, emplaced with a top-to-east displacement. We interpret the mylonitic contact zone between the mafic unit and the basement as a thrust zone,

which has been subsequently folded during the D_2 event.

The stratoid granites emplaced at 630 Ma (Paquette and Nédélec, 1998) do not intrude the Andriamena unit, suggesting that nappe overthusting (D_1 event) occurred after 630 Ma. Monazite ages associated with D_1 structures (flat-lying foliation (sample C98) and the mylonite contact (sample C70) range from about 530 to 460 Ma. The age of 499 ± 19 Ma recorded in euhedral monazites from migmatite C98 is interpreted as the age of partial melting which is also coeval with the development of the S_1 foliation under minimal *P–T* conditions of about 5 kbar and 700 °C. Near the the main tectonic contact, overgrowths of middle Neoproterozoic monazites (724 ± 5 Ma) from sample B39, yield a youngest age of 457 ± 7 Ma. Petrologic observations indicate that the mylonite deformation occurred under epidote-amphibolite-facies conditions (∼500 °C) and probably until lower temperature. Thus, the 457 Ma age is interpreted as a cooling age or as resulting from late fluid circulation, following the nappe emplacement. In contrast, the poorly constrained age of 526 ± 17 Ma, recorded in the rims of the Neoproterozoic monazites could correspond to the initial mylonite deformation (i.e. the nappe emplacement).

5.2. D_2 event: Cambrian east-west horizontal shortening

5.2.1. The D_2 event in the Andriamena unit

The finite strain pattern of the Andriamena unit results from partial overprinting of the earlier D_1 structures by late north-south upright folding (F_2) and local transposition of the gneissic layering (S_1) into a new penetrative north-south vertical foliation (S_2) (Fig. 12). Structures related to this D_2 event are consistent with an east-west horizontal shortening. Such D_2 shortening gives rise to strain partitioning between high-strain zones bounding large domains where the D_1 structures are better preserved. The formation of large-scale dome-and-basin structures near the eastern boundary of the Andriamena unit is also related to the D_2 event. We suggest that such dome-and-basin pattern could result from the combination of type I fold-interference structures with minor gravitational instabilities, according to the high-density contrast between the mafic gneisses of the Andriamena unit and the underlying less dense granites and gneisses of the basement (Fig. 12).

Sample C70 from the D_2 high-strain zone records a late episode of monazite growth (euhedral unzoned grains and secondary overgrowths) and a partial resetting of middle Neoproterozoic monazite (∼730 Ma) at 501 ± 10 Ma. This age is interpreted as the age of the D_2 deformation which is coeval with cooling from about 700 to 600 °C at pressures of 5 ± 1 kbar.

In summary, it appears that metamorphic conditions (amphibolite to granulite conditions) and ages of the D_1 and D_2 event (530–500 Ma) are indistinguishable. We suggest that the eastward thrust emplacement of the Andriamena unit (D_1) followed by the horizontal shortening (D_2) are ascribed to the same Cambrian strain regime (east-west convergence) related to arc convergence and assembly. The east-west shortening is firstly accommodated by sub-horizontal structures (D_1) localized at the boundaries of distinct crustal terranes (Andriamena and gneissic-granitic basement). Then, the strain is accommodated by upright folding and kilometer-scale vertical shear zones (D_2; Angavo shear zone located east of the Andriamena unit) (Fig. 12).

5.2.2. The D_2 event in the basement

In the Andriba area, the occurrence of a kilometer-scale interference pattern is related to the superposition of F_1 folds with open F_2 folds characterized by vertical north-south axial planes and horizontal axes. Foliation map of the Fig. 2 clearly shows that south of the study area (near Ankazobe or the Carion granite), the foliation pattern exhibits kilometer-scale elliptical and tight folded structures corresponding to type I fold-interference patterns (Ramsay, 1967). The main axial traces of these folds are oriented north-south, parallel to the Angavo shear zone and are consistent with the D_2 horizontal shortening. The Carion granite, which is characterized by magmatic to sub-magmatic foliation, without solid state deformation (Madison Razanatseheno, 1998; Nédélec et al., 2000), is concordant with the foliation of the gneissic basement and displays the same N-S structural directions as those observed in the basement (Fig. 2). As proposed by Nédélec et al. (2000), the Carion granite was emplaced in a fold-interference structure, contemporaneous with the last north-south F_2 folding under granulite-facies conditions (∼3 kbar, 750–800 °C).

Numerous geochronologic studies carried out in the basement rocks allow us to constrain the age of the D_2 event. U–Pb SHRIMP dating of the syn-tectonic D_2 Carion granite yields an age of emplacement of 532 ± 5 Ma (Meert et al., 2001) and a Pb–Pb evaporation age of 538 ± 1 Ma (Kröner et al., 2000). The emplacement is followed by a slow cooling constrain by $^{40}Ar/^{39}Ar$ ages on hornblende and biotite at 513 and 479 Ma, respectively (Meert et al., 2001). Numerous charnockites and granites from the Antananarivo area yield U–Th–Pb electron microprobe monazite ages of about 500 Ma (Ramasiarinoro, 1998). Kröner et al. (2000) dated granulite-facies metamorphism that affects the basement close to 550 Ma. All these ages constrain the deformation in the basement at about 550–500 Ma, which is in good agreement with the age obtained from the Andriamena unit.

The north-south Angavo shear zone, located to the east of the Andriamena unit and the Antananarivo virgation, has been interpreted as the northern extension of the Ifanadiana shear zone in the south east Madagascar (Fig. 1; Martelat, 1998). Martelat et al. (2000) interpreted it to have formed by east-west horizontal shortening in a transpressive regime under granulitic-facies conditions at 530–500 Ma.

6. Discussion and conclusions

Combined structural, petrological and geochronological data allow us to constrain the Cambrian tectonic evolution of a part of north-central Madagascar around the Andriamena unit. The basement in this area is mainly composed of late Archaean and middle Neoproterozoic rocks, which have been strongly reworked during the Cambrian. The tectonic evolution consists of two superposed tectonic episodes D_1 and D_2.

The first one (D_1) is related to the thrust emplacement of the Andriamena unit on top of the gneissic-granitic basement with a top-to-east displacement at about 530–500 Ma under amphibolite to granulite-facies conditions. The Andriamena unit, which is characterized by mafic bodies unknown in the surrounding gneissic-granitic basement, is thus allochthonous and was originally located west of its present position. The mafic-ultramafic intrusions dated at 790 Ma are interpreted as the juvenile products of a continental arc magmatism related to the closure of the Mozambique Ocean during the middle Neoproterozoic (Guérrot et al., 1993; Handke et al., 1999; Tucker et al., 1999). Therefore, we suggest that the Andriamena unit corresponds to a fragment of the lower continental magmatic arc, which has been thrusted upon the gneissic-granitic basement at 530–500 Ma.

The second tectonic episode (D_2) is related to an east-west horizontal shortening at ~500 Ma, contemporaneous with amphibolitic to granulitic-facies metamorphism. Such final east-west shortening has been widely recognized in southern Madagascar and in central Madagascar (SQC unit; Lardeaux et al., 1999; Martelat et al., 1997, 2000; Fernandez et al., in press). In southern Madagascar, this tectonic event is coeval with granulite-facies conditions and affects a large part of the lower crust, from 12 to 5 kbar (Martelat et al., 2000). In central Madagascar, it is contemporaneous with greenschist-facies conditions corresponding to an uppermost crustal level (Fernandez et al., in press). The recognition of the D_2 bulk strain pattern, at the scale of Madagascar and at various structural levels of the crust, suggests that the D_2 event results from the final amalgation of Gondwana during late Neoproterozoic–Cambrian collision of the Australia–Antarctica block with the rest of Gondwana (Madagascar, southern India, and Sri Lanka).

Acknowledgements

This work was financially supported by the “Service des Relations Internationales” from Université Blaise Pascal. We acknowledge the © CNES 96-99—distribution Spot Image and the ISIS9912-5 program for the SPOT satellite images. Many thanks are due to V. Ramasiarinoro, N. Ramiandrisoa, and R. Rakotondrazafy for their support in the field, and to M. Veschambre for technical assistance during the electron microprobe work. Helpful and useful reviews of Alan Collins and Rónadh Cox have been greatly appreciated. Finally we are also grateful to T.M. Kusky, M. Abdelsalam, R. Tucker, and R. Stern for the invitation to contribute to this special volume.

References

Andriamarofahatra, J., Boisse, H.D.L., Nicollet, C., 1990. Datation U–Pb sur monazites et zircons du dernier épisode tectono-métamorphique granulitique majeur dans le Sud-Est de

Madagascar. Comptes Rendus de l'Académie des Sciences de Paris 310, 1643–1648.

Berman, R.G., 1991. Thermobarometry using multi-equilibrium calculations: a new technique, with petrological applications. Canadian Mineral. 29, 833–856.

Bésairie, H., 1963. Description géologique du massif ancien de Madagascar. Premier volume Centre Nord et Centre Nord-Est, Service Géologique Tananarive.

Caen-Vachette, M., 1979. Le Précambrien de Madagascar. Radiochronométrie par isochrones Rb/Sr sur roches totales. Revue de géologie dynamique et de géographie physique 21, 331–338.

Cocherie, A., Guérrot, C., Ohnenstetter, M., 1991. Contraintes géochimiques (terres rares et isotopes du néodyme) sur l'origine et l'évolution des complexes ultra-basiques pan-africains de Madagascar (W-Andriamena). Principaux résultats scientifiques et techniques du BRGM, pp. 97–99.

Collins, A.S., Razakamanana, T., Windley, B.F., 2000. Neoproterozoic extensional detachment in central Madagascar: implications for the collapse of the East African Orogen. Geol. Magazine 137, 39–51.

Collins, A.S., Windley, B.F., in press. The tectonic evolution of central and northern Madagascar and its place in the final assembly of gondwana. J. Geol.

de Wit, M.J., Bowring, S.A., Ashwal, L.D., Randrianasolo, L.G., Morel, V.P.I., Rambeloson, R.A., 2001. Age and tectonic evolution of Neoproterozoic ductile shear zone in southwestern Madagascar, with implications for Gondwana studies. Tectonics 20, 1–45.

Fernandez, A., Huber, S., Schreurs, G., in press. Tectonic evolution of the Itremo Region (central Madagascar) and implications for Gondwana assembly. Geol. Magazine.

Ferry, J.M., Spear, F.S., 1978. Experimental calibration of the partitioning between biotite and garnet. Contrib. Mineral. Petrol. 66, 113–117.

Goncalves, P., Nicollet, C., Lardeaux, J.M., 2000. In-situ electron microprobe monazite dating of the complex retrograde evolution of UHT granulites from Andriamena (Madagascar): apparent petrographical path vs. PTt path. Geological Society of America, Annual Meeting, Reno, USA.

Goncalves, P., Nicollet, C., Montel, J.M., Lefevre, B., Paquette, J.L., Lardeaux, J.M., Pin, C., 2001. Is the petrographical PTt path consistent with the real thermal path? The example of the polymetamorphic ultra-high temperature granulites of Andriamena (Madagascar). EUG XI, Strasbourg, France. J. Conf. Abstr. 6, 376.

Guérrot, C., Cocherie, A., Ohnenstetter, M., 1993. Origin and evolution of the West Andriamena Pan-African mafic-ultramafic complex in Madagascar as shown by U–Pb, Nd isotopes and trace element constraints. Terra Abstr. 5, 387.

Handke, M.J., Tucker, R.D., Ashwal, L.D., 1999. Neoproterozoic continental arc magmatism in west-central Madagascar. Geology 27, 351–354.

Hodges, K.V., Crowley, P.D., 1985. Error estimation and empirical geothermobarometry for pelitic systems. Am. Mineral. 70, 702–709.

Koziol, A.M., 1989. Recalibration of the garnet-plagioclase-Al_2SiO_5-quartz (GASP) geobarometer and application to natural parageneses. EOS Transactions (American Geophysical Union) 70, 493.

Kröner, A., Braun, I., Jaeckel, P., 1996. Zircon geochronology of anatectic melts and residues from high-grade pelitic assemblages at Ihosy, southern Madagascar: evidence for Pan-African granulite metamorphism. Geol. Magazine 133, 311–323.

Kröner, A., Hegner, E., Collins, A.S., Windley, B.F., Brewer, T.S., Razakamanana, T., Pidgeon, R.T., 2000. Age and magmatic history of the Antananarivo block, central Madagascar, as derived from zircon geochronology and Nd isotopic systematics. Am. J. Sci. 300, 251–288.

Lardeaux, J.M., Martelat, J.E., Nicollet, C., Rakotondrazafy, R., Cardon, H., 1999. Metamorphism and tectonics in southern Madagascar: an overview. Gondwana Res. 2, 355–362.

Madison Razanatseheno, M.O., 1998. Granite de Carion: approches pétrologiques et structurales. MSc Thesis, Université d'Antananarivo, Madagascar.

Martelat, J.E., 1998. Evolution Thermomécanique de la croûte inférieure du Sud de Madagascar. Ph.D. Thesis, Université Blaise Pascal—Clermont-Ferrand II, France.

Martelat, J.E., Lardeaux, J.M., Nicollet, C., Rakotondrazafy, R., 1999. Exhumation of granulites within a transpressive regime: an example from southern Madagascar. Gondwana Res. 2, 363–367.

Martelat, J.E., Lardeaux, J.M., Nicollet, C., Rakotondrazafy, R., 2000. Strain pattern and late Precambrian deformation history in southern Madagascar. Precambrian Res. 102, 1–20.

Martelat, J.E., Nicollet, C., Lardeaux, J.M., Vidal, G., Rakotondrazafy, R., 1997. Lithospheric tectonic structures developed under high-grade metamorphism in the southern part of Madagascar. Geodinam. Acta 10, 94–114.

Meert, J.G., Van der Voo, R., 1997. The assembly of Gondwana 800–550 Ma. J. Geodynam. 23, 223–235.

Martelat, J.E., Vidal, G., Lardeaux, J.M., Nicollet, C., Rakotondrazafy, R., 1995. Satellite images and tectonics of the lower continental crust: The example of south-western Madagascar. Comptes Rendus de l'Académie des Sciences de Paris 321, 325–332.

Meert, J.G., Nédélec, A., Hall, C., Wingate, M.T.D., Rakotondrazafy, M., 2001. Paleomagnetism, geochronology and tectonic implications of the Cambrian-age Carion granite, central Madagascar. Tectonophysics 340, 1–21.

Montel, J.M., Foret, S., Veschambre, M., Nicollet, N., Provost, A., 1996. Electron microprobe dating of monazite. Chem. Geol. 131, 37–53.

Nédélec, A., Paquette, J.L., Bouchez, J.L., Olivier, P., Ralison, B., 1994. Stratoid granites of Madagascar: structure and position in the Pan-African Orogeny. Geodinam. Acta 7, 48–56.

Nédélec, A., Ralison, B., Bouchez, J.L., Grégoire, V., 2000. Structure and metamorphism of the granitic basement around Antananarivo: a key to the Pan-African history of central Madagascar and its Gondwana connections. Tectonics 19, 997–1020.

Nédélec, A., Stephens, W.E., Fallick, A.E., 1995. The panafrican stratoid granites of Madagascar: alkaline magmatism in a post-collisional extensional setting. J. Petrol. 36, 1367–1391.

Nicollet, C., 1988. Metabasites granulitiques, anorthosites et roches associées de la croûte inférieure: Exemple pris à Madagascar et dans le Massif Central Français. Arguments en faveur d'un métamorphisme associé à l'extension lithosphérique. Thèse d'Etat, Université Blaise-Pascal, Clermont-Ferrand, France.

Nicollet, C., 1990. Crustal evolution of the granulites of Madagascar. In: Vielzeuf, D., Vidal, P. (Eds.), Granulites and Crustal Evolution. Kluwer Academic publishers, Dodrecht, pp. 391–310.

Nicollet, C., Montel, J.M., Foret, S., Martelat, J.E., Rakotondrazafy, R., Lardeaux, J.M., 1997. E-probe monazite dating in Madagascar: a good example of the usefulness of the in-situ dating method. UNESCO-IUGS-IGCP 348/368. In: Proceedings of the Internal Symposium and Field Workshop on Proterozoic Geology of Madagascar, pp. 65.

Paquette, J.L., Nédélec, A., 1998. A new insight into Pan-African tectonics in the East-West Gondwana collision zone by U–Pb zircon dating of granites from central Madagascar. Earth Planet. Sci. Lett. 155, 45–56.

Paquette, J.L., Nédélec, A., Moine, B., Rakotondrazafy, M., 1994. U–Pb, single zircon Pb-evaporation, and Sm–Nd isotopic study of a granulite domain in SE Madagascar. J. Geol. 102, 523–538.

Pili, E., Ricard, Y., Lardeaux, J.M., Sheppard, S.M.F., 1997. Lithospheric shear zones and mantle-crust connections. Tectonophysics 280, 15–29.

Ramasiarinoro, V.J., 1998. Etudes des charnockites et granitoïdes des environs d'Antananarivo. MSc Thesis, Université d'Antananarivo, Madagascar.

Ramsay, J.G., 1967. Folding and Fracturing of Rocks. McGraw-Hill, New-York.

Spear, F.S., 1999. Real-time AFM diagrams on your Macintosh. Geol. Mater. Res. 1, 1–18.

Spear, F.S., Kohn, M.J., Cheney, J.T., 1999. *P–T* paths from anatectic pelites. Contrib. Mineral. Petrol. 134, 17–32.

Stern, R.J., 1994. Arc assembly and continental collision in the Neoproterozoic East African Orogen: Implications for the consolidation of Gondwanaland. Annu. Rev. Earth and Planet. Sci. 22, 319–351.

St-Onge, M.R., Ijewliw, O.J., 1996. Mineral corona formation during high-P retrogression of granulitic rocks, Ungava Orogen, Canada. Contrib. Mineral. Petrol. 37, 553–582.

Tucker, R.D., Ashwal, L.D., Handke, M.J., Hamilton, M.A., Grange, M.L., Rambeloson, R.A., 1999. U–Pb geochronology and isotope geochemistry of the Archean and Proterozoic rocks of north-central Madagascar. J. Geol. 107, 135–153.